The magnitude of the intrinsic rate constant: How deep can association reactions be in the diffusion limited regime?

Vijaykumar, A.; ten Wolde, P.R.; Bolhuis, P.G.

DOI
10.1063/1.5009547

Publication date
2017

Document Version
Final published version

Published in
Journal of Chemical Physics

The magnitude of the intrinsic rate constant: How deep can association reactions be in the diffusion limited regime?

Adithya Vijaykumar,[1,2] Pieter Rein ten Wolde,[1,a)] and Peter G. Bolhuis[2,b)]
[1]*FOM Institute AMOLF, Science Park 104, 1098 XG Amsterdam, The Netherlands*
[2]*Van 't Hoff Institute for Molecular Sciences, University of Amsterdam, P.O. Box 94157, 1090 GD Amsterdam, The Netherlands*

(Received 13 April 2017; accepted 4 October 2017; published online 10 November 2017)

Intrinsic and effective rate constants have an important role in the theory of diffusion-limited reactions. In a previous paper, we provide detailed microscopic expressions for these intrinsic rates [A. Vijaykumar, P. G. Bolhuis, and P. R. ten Wolde, Faraday Discuss. **195**, 421 (2016)], which are usually considered as abstract quantities and assumed to be implicitly known. Using these microscopic expressions, we investigate how the rate of association depends on the strength and the range of the isotropic potential and the strength of the non-specific attraction in case of the anisotropic potential. In addition, we determine the location of the interface where these expressions become valid for anisotropic potentials. In particular, by investigating the particles' orientational distributions, we verify whether the interface at which these distributions become isotropic agrees with the interface predicted by the effective association rate constant. Finally, we discuss how large the intrinsic association rate can become, and what are the consequences for the existence of the diffusion limited regime. *Published by AIP Publishing.* https://doi.org/10.1063/1.5009547

I. INTRODUCTION

Association and dissociation of pairs of particles play a central role not only in cellular processes such as the binding of a ligand to a receptor, an enzyme to its substrate, or a protein to DNA in gene regulation but also in the self-assembly of colloids, in micro-emulsion formation or in the phase behavior of polymer solutions. During association, particles come into contact via diffusion and bind with a rate depending on the intrinsic association rate constant. When dissociating, a bound particle pair separates with an intrinsic dissociation rate, after which the particles diffuse away from each other. Theories of diffusion-influenced reactions express the experimentally important *effective* rate constants in terms of diffusion constants, cross section, interaction potential of the particles, and the intrinsic association and dissociation rate constants.[1] The latter are often assumed as *a priori* given.

While simulation techniques exist that can compute association and dissociation rate constants for arbitrarily complex interaction potentials,[2,3] these are typically *effective* rate constants, resulting from both the diffusion process and the binding rate upon contact due to the interaction potential. Since the effective rate is also what is often measured in experiments, few studies have focused on the dependence of intrinsic rate constants on the interaction potential, the cross section, and the particles' diffusion constants.

Knowledge of the effective association and dissociation rates is sufficient for describing the dynamics of dilute systems when the association and dissociation can be reduced to a two-body problem. Yet, it should be realized that, in general, association-dissociation reactions present a complicated non-Markovian many-body problem due to non-trivial spatio-temporal correlations between the reactions, such as rebinding events. In dilute systems, it is often possible to integrate out the dynamics at the molecular scale and describe association-dissociation as a Markovian process with effective rates describing the long time dynamics.[4,5] However, the evidence is accumulating that even in dilute systems, molecular-scale spatio-temporal correlations can dramatically influence the system's macroscopic scale behavior. For example, it has been predicted[6,7] and shown by experiments[8] that in cellular systems which rely on multi-site protein modification, enzyme-substrate rebindings at the microscopic scale can dramatically change the macroscopic behavior at the cellular scale. Also in chemical sensing, either by living cells or man-made sensors,[9–14] the accuracy of sensing is affected by the microscopic dynamics of the ligand binding to and hopping between multiple receptors. In these cases, the effective rate constants are not sufficient for describing the dynamics: instead, this requires knowledge of diffusion constants, the cross sections, and the intrinsic rate constants. Also for the modeling of reactions in spatially heterogeneous cellular systems as well as in confined geometries or reduced dimensions, knowledge of the intrinsic rate constants is required. In addition, in recent years, much effort has been devoted to understanding how the accuracy of sensing is set by the diffusion-limited arrival of the ligand at the receptor.[5,9–13,15–17] However, the limit derived is only tight if the ligand-receptor association reactions are indeed diffusion limited, meaning that the intrinsic rate constant is much larger than the diffusion-limited rate constant. Last but not least, knowledge of

[a)]Electronic mail: p.t.wolde@amolf.nl
[b)]Electronic mail: p.g.bolhuis@uva.nl

intrinsic rates is essential for simulation techniques that model (bio)chemical networks of chemical reactions via reaction-diffusion, in which particles move by diffusion, and react at contact with a *given* intrinsic rate constant.[6,18–25]

In Ref. 24, we derived microscopic expressions for these intrinsic rates that can be evaluated by focusing on a single dissociation reaction using a rare-event sampling technique. We demonstrated that these expressions not only hold for generic isotropic potentials but also for anisotropic potentials, provided the cross section where the intrinsic rates are calculated is sufficiently far from contact that the particles' orientational distributions are isotropic.

In this work, we use the technique introduced in Ref. 24 to study the intrinsic and effective rate constants as a function of the parameters of both isotropic and anisotropic (patchy) interaction potentials. For the isotropic potential, we use the potential introduced in Ref. 26, which can accurately describe the phase behavior of small globular proteins such as lysozyme. For this potential, we investigate how the intrinsic and effective rate constants vary with the strength and the range of the interaction potential. For the anisotropic potential, we use the potential introduced in Ref. 24, which provides an effective coarse-grained model for proteins with patchy binding sites. The particles experience a repulsive force based on the distance between their centres of mass and a strong specific attractive force if their patches are aligned. In addition, particles also experience a weaker, isotropic attractive force, which models the non-specific binding in proteins. Besides the bound and unbound states, this isotropic non-specific attraction facilitates an intermediate weakly bound state, in which the particles are not bound to a specific patch but are likely to remain close to each other, increasing the chances that they rebind to a patch. We compute for this system how the intrinsic and effective rate constants vary with the non-specific attraction strength. Since the expressions for the rates derived in Ref. 24 are valid for the anisotropic potential only at cross sections sufficiently far from contact, we also determine the interface where the orientational distributions become isotropic as a function of the non-specific attraction strength. While previous work has considered association and dissociation for isotropic interactions,[1,14,27,28] as well as association for anisotropic interactions,[2,29] these above issues have not been considered before.

The article is organized as follows: In Sec. II, we present a brief derivation of the expressions for the rate constants using rare-event sampling techniques, followed by a short description of the particle model and the interaction potential and the methods that are used to perform the simulations. In Sec. III, we evaluate these rates for the isotropic potential, varying its range and strength. Not surprisingly, the intrinsic and effective association rates increase with the interaction strength, while the corresponding dissociation rates strongly decrease. More interestingly, the intrinsic and effective association rates fall as the interaction range decreases, while the corresponding dissociation rate constants increase. We then determine the cross section beyond which these expressions hold for anisotropic potentials and calculate the anisotropic rates as a function of the non-specific attraction strength. The results show that non-specific binding can significantly speed up association and slow down dissociation. We end with the conclusion in Sec. IV where we discuss the question how deep the association process can be in the diffusion limited regime. For the potentials studied here, the intrinsic association rate is about a factor 10 higher than the effective rate constant, which means that the overall association speed is more limited by diffusion than by the binding rate at contact but certainly is not entirely dominated by it.

II. METHODS

A. Intrinsic and effective rate constants

In this section, we briefly recapitulate the derivation that led up to the expressions for the intrinsic rate constants.[24] The central quantities in a reaction-diffusion system, as shown in Fig. 1, are as follows: (i) the relative diffusion constant, D, which is the diffusion constant associated with the interparticle vector of the two associating species A and B: $D = D_A + D_B$, where D_A and D_B are the diffusion constants of the respective particles;[6,30] (ii) the cross section σ, this cross section is the "contact distance" at which the particles can associate with each other; (iii) the intrinsic association rate, k_a, at which the particles can go from the contact state to the bound state; (iv) the intrinsic dissociation rate, k_d, at which the particles can unbind from the bound state to the contact state; (v) the interaction potential $U(r)$.

When the interaction potential $U(r)$ is zero beyond the constant distance σ, the rate at which the particles come into contact, starting from an equilibrium distribution, is given by the diffusion-limited rate constant, $k_D = 4\pi\sigma D$. In this case, the long-time limit of the time-dependent association rate is given by the effective association rate given by the Collins-Kimbal rate constant,[27]

$$k_{\mathrm{on}} = k_{\mathrm{D}}(\sigma).\frac{k_{\mathrm{a}}(\sigma)}{k_{\mathrm{a}}(\sigma) + k_{\mathrm{D}}(\sigma)}. \tag{1}$$

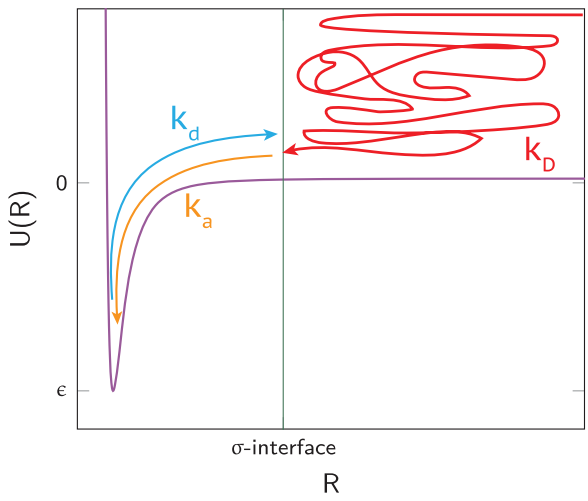

FIG. 1. Central quantities in a reaction-diffusion system. Particles from an equilibrium distribution arrive at the contact interface, σ, with a diffusion limited rate, k_{D}. In the case of particles freely diffusing with a diffusion constant D, the analytical expression for the diffusion limited rate, $k_{\mathrm{D}} = 4\pi\sigma D$. From contact, the particles can go to the bound state with an intrinsic association rate, k_{a}, and once bound, the particles can unbind with an intrinsic dissociation rate, k_{d}. R is the inter-particle distance and $U(R)$ is the interaction potential.

This expression shows that the effective association rate k_{on} can be interpreted as the rate at which particles come into contact, $k_D(\sigma)$, multiplied by the probability that, given they are in contact, they subsequently also react, $k_a(\sigma)/(k_a(\sigma) + k_D(\sigma))$. We also emphasize that while k_{on} is independent of the choice of the contact distance σ, k_a and k_D do depend on this choice.

In the same limit $U(r = 0)$ for $r > \sigma$, the effective dissociation rate as derived by Berg[28] is given by

$$k_{off} = k_d(\sigma).\frac{k_D(\sigma)}{k_a(\sigma) + k_D(\sigma)}. \quad (2)$$

The effective dissociation rate k_{off} is thus the rate at which the bound particles dissociate, $k_d(\sigma)$, times the probability that they subsequently escape to infinity. While the effective dissociation rate k_{off} is independent of the choice of σ, the intrinsic dissociation rate $k_d(\sigma)$ does depend on it.

Dissociation is a rare event when particles are bound to patches, owing to strong specific attractive forces. Rare event sampling techniques such as Transition Interface Sampling[31] (TIS) or Forward Flux Sampling[32,33] (FFS) allow evaluation of the corresponding low rate constants. The effective dissociation rate k_{off} can be expressed as $k_{off} = \Phi_0 P(\infty|r_0)$, where Φ_0 is the flux of trajectories coming from the bound state and crossing the r_0-interface for the first time and $P(\infty|r_0)$ is the conditional probability for trajectories starting at the r_0-interface to reach infinity (unbound state), instead of returning back to the bound state. This probability of escaping to the unbound state from the r_0-interface can in turn be written as the probability of escaping from the bound state to the σ-interface first, multiplied by the probability of subsequently escaping to the unbound state from the σ-interface. It follows that

$$k_{off} = \Phi_0 P(\sigma|r_0) P(\infty|\sigma). \quad (3)$$

Note that this expression is exact[31] and applies to any interaction potential. More specifically, it does not require that $U(r)$ is zero beyond the cutoff distance σ. The first two terms of Eq. (3) can be recognized as the definition of the intrinsic dissociation rate constant

$$k_d = \Phi_0 P(\sigma|r_0), \quad (4)$$

which makes it possible to write the effective dissociation rate constant as

$$k_{off} = k_d P(\infty|\sigma). \quad (5)$$

This expression is also exact, applying even when $U(r)$ is non-zero beyond σ. However, if the contact distance σ is chosen beyond the cutoff distance where the potential becomes zero, then we can combine Eq. (5) with Eq. (2) to express the escape probability in terms of the intrinsic association rate and the diffusion-limited rate constant

$$P(\infty|\sigma) = \frac{k_D(\sigma)}{k_a(\sigma) + k_D(\sigma)}. \quad (6)$$

Rearranging leads to an expression for the intrinsic association rate

$$k_a(\sigma) = k_D(\sigma)\frac{1 - P(\infty|\sigma)}{P(\infty|\sigma)}. \quad (7)$$

$P(\infty|\sigma)$ could in principle be obtained by performing a single TIS/FFS simulation for the dissociation reaction. Hence, by putting σ beyond the cutoff distance of the potential and by exploiting the analytical expressions for the diffusion-limited rate, $k_D(\sigma) = 4\pi\sigma$, and the escape probability, $P(\infty|\sigma) = k_D(\sigma)/(k_a(\sigma) + k_D(\sigma)$, we can, from one TIS/FFS simulation of a dissociation reaction, not only obtain the intrinsic rate $k_d(\sigma)$, via Eq. (4), and the effective dissociation rate k_{off}, via Eq. (5), but also the intrinsic association rate $k_a(\sigma)$, via Eq. (7), and the effective association rate k_{on}, via Eq. (1). Indeed, in all analyses performed below, we always put the cross section beyond the cutoff of the potential (Fig. 2).

$P(\infty|\sigma)$ cannot be computed directly within a FFS/TIS simulation because the last interface cannot be put at infinity in practice. In the simulations, we thus put the last interface at a finite distance r_n, and compute $P(r_n|\sigma)$ instead. However, we then need a correction because the particles can rebind; in fact, even when r_n is chosen to be large, we still need this correction because the rebinding probability decays, as we will see, very slowly only with r_n, namely, as $1/r_n$. To relate $P(\infty|\sigma)$ to $P(r_n|\sigma)$, we exploit that the effective rate constants are independent of the choice of the dividing interface, $k_{on}(\sigma) = k_{on}(r_n)$ so that

$$k_D(\sigma)(1 - P(\infty|\sigma)) = k_D(r_n)(1 - P(\infty|r_n)), \quad (8)$$

where $1 - P(\infty|\sigma) = k_a(\sigma)/(k_a(\sigma) + k_D(\sigma))$ is the splitting probability for binding [c.f. Eq. (1)]. Factorizing $P(\infty|\sigma)$ as

$$P(\infty|\sigma) = P(\infty|r_n)P(r_n|\sigma) \quad (9)$$

and simultaneously solving Eqs. (8) and (9) yield expressions for $P(\infty|r_n)$ and $P(\infty|\sigma)$. Substituting the expression of $P(\infty|\sigma)$ in Eq. (7) gives

$$k_a(\sigma) = k_D(\sigma)\frac{1 - P(r_n|\sigma)}{P(r_n|\sigma)}\left(1 - \frac{k_D(\sigma)}{k_D(r_n)}\right)^{-1}. \quad (10)$$

Thus for a r_n-interface chosen at a finite distance, we need to correct k_a by dividing through a factor $(1 - k_D(\sigma)/k_D(r_n))$. The only unknown $P(r_n|\sigma)$ follows directly from the FFS/TIS

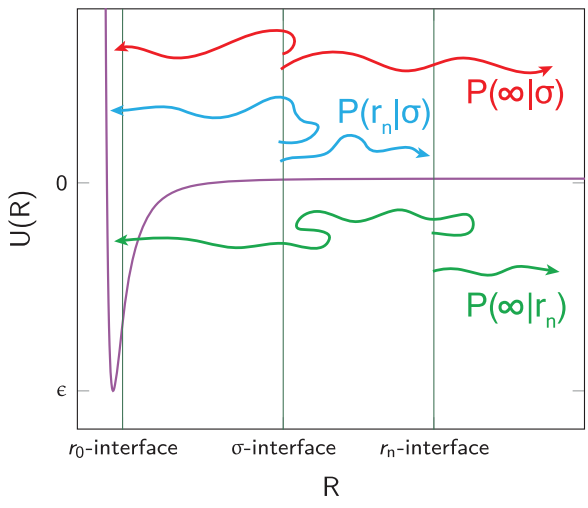

FIG. 2. The main interfaces used in the FFS/TIS simulation to calculate the rate constants. Particles within the r_0-interface are in a bound state and beyond the r_n-interface are in the unbound state. The σ-interface which is in between the r_0 and r_n interfaces is the cross section where the particles are at contact. The conditional probabilities in the case of FFS/TIS are the probability of going from one interface to the next, as opposed to going back to r_0. R is the inter-particle distance and $U(R)$ is the interaction potential.

simulation (Fig. 2). This procedure can also be used to calculate the rate constants for particles interacting with anisotropic potentials, provided the position of the interface where these rates are measured is sufficiently far from contact such that the orientational distributions on this interface are isotropic.[24] Consider an interface, σ', which is sufficiently far from contact such that the distribution of trajectories has become uniform. The intrinsic rate for that surface is given by Eq. (10),

$$k_a(\sigma') = k_D(\sigma')\frac{1 - P(r_n|\sigma')}{P(r_n|\sigma')}\left(1 - \frac{k_D(\sigma')}{k_D(r_n)}\right)^{-1}. \quad (11)$$

Since we know that the effective association rate is independent of the choice of the dividing surface, we can write

$$\frac{1}{k_{on}} = \frac{1}{k_a(\sigma)} + \frac{1}{k_D(\sigma)} = \frac{1}{k_a(\sigma')} + \frac{1}{k_D(\sigma')}, \quad (12)$$

even if the distribution at σ is anisotropic. Inserting Eq. (11) into Eq. (12) yields

$$k_a(\sigma) = \frac{(1 - P(r_n|\sigma'))k_D(\sigma')k_D(\sigma)}{P(r_n|\sigma')(k_D(\sigma') - k_D(\sigma)\Omega) + k_D(\sigma) - k_D(\sigma')}, \quad (13)$$

where $\Omega = \sigma'/r_n$. This equation reduces to Eq. (10) when $\sigma = \sigma'$. Using Eq. (13) in Eq. (12), we get

$$k_{on} = \frac{(1 - P(r_n|\sigma'))\, k_D(\sigma')}{1 - \Omega P(r_n|\sigma')}. \quad (14)$$

We showed in Ref. 24 that the value of k_{on} as a function of σ' becomes constant beyond $\sigma' > 3\sigma_{an}$ for a non-specific interaction strength $\epsilon_{ns} = 10k_BT$ and predicted that at this interface the orientational distributions of the particles become isotropic. We also showed in Ref. 24 that it is still possible to extract a meaningful value for the intrinsic rate constant at cross sections $\sigma < \sigma'$ by using Eq. (13).

In this paper, we study how the interface at which the distributions become isotropic changes as a function of the strength of the non-specific attraction.

B. Particle models and interaction potentials

We employ two models of particles: (i) spherical particles interacting via an isotropic interaction potential between their centres of mass; (ii) spherical particles with an isotropic centre of mass interaction, dressed with one or more sticky spots on their surface called "patches," which allow for highly directional, anisotropic interactions. In Subsections II B 1–II B 2, we describe the isotropic and anisotropic potentials used to calculate the rate constants.

1. Isotropic potential

For the isotropic interaction, we use the Lennard-Jones-inspired potential from Ref. 26, which allows easy control of the interaction range

$$U_i(R) = \frac{4\epsilon}{\alpha^2}\left(\left[\left(\frac{R}{\sigma_i}\right)^2 - 1\right]^{-6} - \alpha\left[\left(\frac{R}{\sigma_i}\right)^2 - 1\right]^{-3}\right), \quad (15)$$

where R is the centre-of-mass distance between the particles. This potential diverges asymptotically at $R = \sigma_i$, as opposed to the 12-6 LJ potential, which asymptotically diverges at $R = 0$. The strength of interaction is set by ϵ and the interaction range by α. A larger value of α means a smaller interaction range. Figure 3 shows the potential for three values of $\alpha = \{50, 100, 1000\}$ as a function of R, each plotted for two different interaction ranges ($\epsilon = 5k_BT$ and $10k_BT$). In our simulations, $\sigma_i = 5$ nm, roughly corresponding to a protein's diameter. For the sake of comparison, we also plot the standard 12-6 Lennard-Jones interaction, given by

$$U_{LJ}(R) = 4\epsilon\left[\left(\frac{\sigma_{LJ}}{R}\right)^{12} - \left(\frac{\sigma_{LJ}}{R}\right)^{6}\right]. \quad (16)$$

Note that this standard LJ potential is indeed much longer ranged.

2. Anisotropic potential

Patchy particles [illustrated in Fig. 4(a)] can model proteins in an (idealized) coarse-grained way, where the patches represent the binding sites on the protein. Pairs of patchy particles, in our model, experience a strong attractive potential, $U_s(r)$, over a narrow band of orientations [see Fig. 4(c)]. This specific attraction depends on the distance, r, between the patches, i.e., stronger attraction when the patches are closer. When the patchy particles approach each other, they experience a repulsive potential, $U_{rep}(R)$, which is a function of the center-of-mass distance, R. In addition, particles experience a weak, isotropic, non-specific attraction, $U_{ns}(R)$. The total patch potential reads

$$U_{an}(R, r) = U_s(r) + U_{rep}(R) + U_{ns}(R), \quad (17)$$

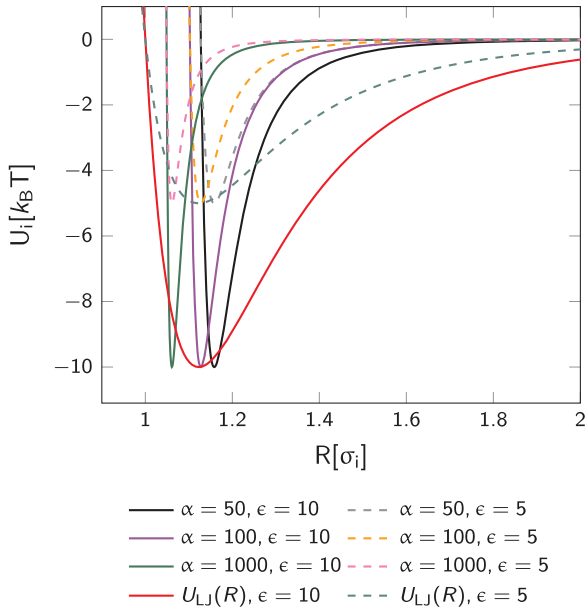

FIG. 3. The isotropic potential, U_i [Eq. (15)], as a function of the inter-particle distance R. The range and the interaction strength of the potential are set by α and ϵ, respectively. A larger value of α results in a potential with a smaller range. The isotropic is the potential plotted for three ranges ($\alpha = \{1000, 100, 50\}$) each with two different attraction strengths ($\epsilon = 5k_BT$ and $10k_BT$). The 12-6 Lennard-Jones potentials have also been plotted for comparison. The intrinsic and effective association and dissociation constants are evaluated for these six cases.

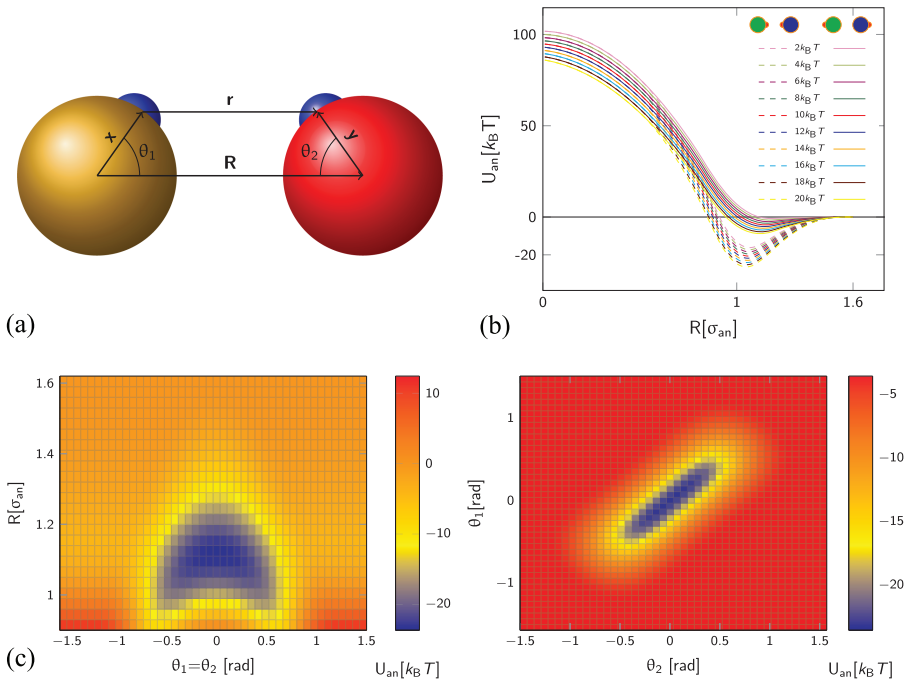

FIG. 4. (a) Particles interacting via the anisotropic potential have sticky spots on the surface called "patches." These patches facilitate highly directional attractive interactions, which provide an effective model for proteins with binding sites. Particles interact via a combination of a repulsive force based on the centre-of-mass distance, R, between the particles and a strong attractive force based on the distance between patches, r. In addition to this, particles experience a centre-of-mass distance based weak, non-specific, attractive force. This non-specific attraction facilitates a weakly bound state causing the particles not to immediately diffuse away once they unbind from the patches. This increases the probability of rebinding of the particles. (b) The anisotropic potential [Eq. (18)] as a function of the inter-particle distance for aligned (dashed line) and misaligned (solid line) patches. The anisotropic potential is plotted for ten different non-specific attraction strengths ($\epsilon_{ns} = 2k_BT$, $4k_BT$, $6k_BT$, $8k_BT$, $10k_BT$, $12k_BT$, $14k_BT$, $16k_BT$, $18k_BT$, $20k_BT$). When the patches are aligned, the distance between the patches is $r = R - \sigma_{an}$, and when misaligned $r = R + \sigma_{an}$, where σ_{an} is the length scale of the anisotropic potential and determines the particles' diameter. (c) Left: Heat map of the anisotropic potential as a function of distance R and the angle between the patch vector and the inter-particle vector, with $\theta_1 = \theta_2$ [angles as defined in (a)]. Right: Heat map of the anisotropic potential as a function of θ_1 and θ_2, for a fixed $R = 1.1\sigma_{an}$. From these heat maps, it follows that the specific attraction is strong only for a narrow range of orientations.

where $U_s(r)$, $U_{rep}(R)$, and $U_{ns}(R)$ have the form

$$U_i(x) = \begin{cases} \epsilon_i \left(1 - a_i \left(\frac{x}{\sigma_{an}}\right)^2\right) & \text{if } x < x_i^\star, \\ \epsilon_i b_i \left(\frac{x_i^c}{\sigma_{an}} - \frac{x}{\sigma_{an}}\right)^2 & \text{if } x_i^\star < x < x_i^c, \\ 0 & \text{otherwise,} \end{cases} \tag{18}$$

with $i = \{s, rep, ns\}$, respectively. The overall strength ϵ_i, the length scale $\sigma_{an} = 5$ nm, the stiffness a_i, and the parameter $x_i^\star$, when combined with a_i determines the range of the potential, are free parameters. Cutoffs x_i^c and smoothing parameters b_i are fixed by requiring continuity and differentiability at $x_i^\star$. In this paper, we set the following parameters: $\epsilon_s = 20k_BT$, $a_s = 20$, and $r_{att}^* = 0.1\sigma_{an}$, implying $b_s = 5$ and $r_s^c = 0.5\sigma_{an}$; $\epsilon_{rep} = 100k_BT$, $a_{rep} = 1$, and $R_{rep}^* = 0.85\sigma_{an}$, implying $b_{rep} = 2.6036$ and $R_{rep}^c = 1.1764\sigma_{an}$; and $a_{ns} = 1$ and $R_{ns}^* = 0.85\sigma_{an}$, implying $b_{ns} = 2.6036$ and $R_{ns}^c = 1.1764\sigma_{an}$. ϵ_{ns} is varied from $2k_BT$ to $20k_BT$ with steps of $2k_BT$. Figure 4(b) shows the total potential as a function of R, when the patches are aligned ($r = R - \sigma_{an}$) and misaligned ($r = R + \sigma_{an}$). When the patches are aligned, particles experience both specific and non-specific attraction, creating a deeper potential well and a stronger bond. When the patches are misaligned, $U_s = 0$ and the particles only experience the weak U_{ns} which results in a shallow potential well and a weaker bond. The non-specific attraction, however, promotes realignment since the particles do not diffuse away immediately.

C. Brownian dynamics of patchy particles

Propagation of the particle dynamics is done with Brownian dynamics, where at each time step δt the particles position and orientation are updated based on the instantaneous total force and torque acting on the particle. This total force/torque on the particle can be divided into three parts: $F_{tot} = F_v + F_p + F_r$. F_v is the viscous drag force, arising from the motion of the particle in a viscous solvent. F_p is the potential force due to interactions between the solute particles, as specified above. F_r is the random force, which models the interaction of the larger solute particles with smaller solvent particles.

In case of anisotropic interactions, the total force and the torque are calculated, where the orientation of the particles is represented using quaternions. We use the Brownian dynamics integrator derived in Ref. 34 to simulate the rotational particle dynamics. Parameters important in this integrator are the temperature T, the time step δt, and the translational and rotational friction coefficients $\gamma = \frac{k_BT}{D_t m}$ and $\Gamma = \frac{k_BT}{D_r M}$, respectively, where D_r and D_t are the translational and rotational diffusion coefficients, respectively, with k_B Boltzmann's constant. The mass of the particle m and the mass moment of inertia M are needed due to the formalism of the algorithm

but drop out during the integration so that the dynamics will not be dependent on inertia. For more details see Refs. 34 and 23–25.

D. Dissociation rates by forward flux sampling

As explained in Sec. II A, evaluation of the rate constants requires simulation of the dissociation reaction. Since dissociation is a rare event, brute force BD is very inefficient, and we have to use a rare event sampling technique such as TIS[31] or FFS. Here we use the "direct-FFS" variant[33] to compute the rate constants. FFS is a simple, computationally efficient and inherently parallel algorithm to obtain good statistics of rare-event kinetics. At heart, FFS uses a series of interfaces between the bound and unbound states to calculate the transition path ensemble and calculate the corresponding transition rate. Trajectories starting in the bound state and reaching the unbound state are rare, but those starting at an interface and reaching the next interface are more common, if the interfaces are placed sufficiently close to each other. The interfaces are defined by a suitable order parameter λ: $(\lambda_0 \ldots \lambda_{n-1})$. FFS assumes that all trajectories from the bound to the unbound state should pass through all the interfaces in succession and that $\lambda_{i+1} > \lambda_i$ for all i. The order parameters used to define the interfaces in FFS are given below.

E. Simulation details

The system specific parameters of the simulation are as follows: The time step $\delta t = 0.1$ ns for the anisotropic potential and $\delta t = 10$ ns for the isotropic potential, the mass of the particle is $m = 50$ kDa, the mass moment of inertia is $M = \frac{8}{15} m\sigma_{an}^2$, the translational and rotational diffusion constants are $D_t = 1$ μm^2/s and $D_r = 1.6 \times 10^7$ rad^2/s for all particles, the translational and rotational friction coefficients are $\gamma = \frac{k_B T}{D_t m}$ and $\Gamma = \frac{k_B T}{D_r M}$, respectively, where $k_B = 1.38 \times 10^{-23}$ J K^{-1} is the Boltzmann constant and $T = 300$ K is the temperature of the system.

For the isotropic potential, the order parameters that define interfaces in the FFS simulation are based on the distance R between the centres-of-mass of the particles. The first interface (r_0-interface), which defines the bound state is at $R = 1.2\sigma_i$. Successive interfaces are placed at $R = 1.3$, 1.4, 1.5, and $1.6\sigma_i$. At $1.6\sigma_i$, the isotropic potential is truncated to zero, and this interface is the σ-interface. Beyond the cutoff, there is only one interface at $R = 2.0\sigma_i$: this is the r_n-interface which is used to compute the escape probability $P(\infty|\sigma)$.

In case of the anisotropic potential, the interfaces are defined in terms of energy, $U_{an}(R, r)$ until the cutoff of the potential, beyond which they are based on the interparticle distance, R. The first interface (r_0-interface) defining the bound state is placed at $18k_BT$. The successive interfaces are located at 15, 10, and $5k_BT$. The σ-interface at the cutoff of the potential is defined by zero energy and $R = 1.6\sigma_{an}$. Beyond the cutoff of the potential, interfaces are placed at $R = 1.7$, 1.9, 2.1, 2.3, 2.5, 3.0, 3.5, 4.0, 4.5, 5.0, 5.5 and finally the r_n-interface is placed at $R = 7\sigma_{an}$.

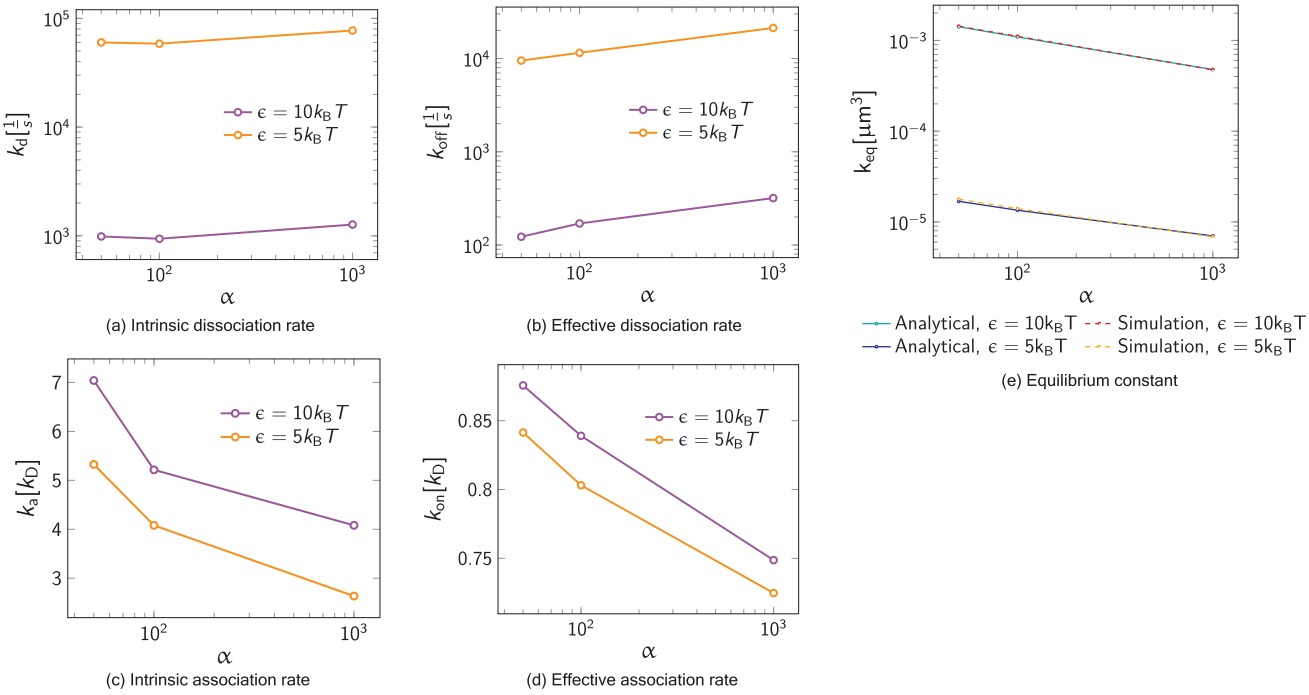

FIG. 5. The intrinsic [(a) and (c)] and effective [(b) and (d)] rate constants and the equilibrium constants (e) as a function of the range of the isotropic potential [see Eq. (15)], plotted for two different values the strength of the potential, $\epsilon = 5k_BT$, $10k_BT$. The range of the potential is set by the parameter α, where a larger value of α results in a potential having a smaller range. The intrinsic rates are calculated at the σ-interface ($R = 1.6\sigma_i$), beyond which the value of the potential is truncated to zero. The values of k_d and k_{off} increase with decreasing range and increasing strength of the potential. The values of k_a and k_{on} decrease with decreasing range and increasing strength of the potential. In panel (e), the equilibrium constant is either calculated via $K_{eq} = k_a/k_d = k_{on}/k_{off}$, where k_a, k_d, k_{on}, and k_{off} are computed via the simulation technique presented in this paper, or analytically, by integrating the interaction potential, see Ref. 23.

III. RESULTS

We calculated the rate constants by systematically varying the strength and the range of interaction for the isotropic potential and the non-specific attraction strength for the anisotropic potential. In the latter case of the anisotropic potential, we also determine, as a function of the non-specific attraction strength, the interface beyond which the expressions of these rate constants are valid.

A. Rate constants for the isotropic potential

We calculate the intrinsic and effective, association and dissociation rates as detailed in Sec. II A for different values of the range (α) and the strength (ϵ) of the isotropic potential. The r_0, σ, and r_n interfaces are at $R = 1.2\sigma_i$, $R = 1.6\sigma_i$, and $R = 2.0\sigma_i$, respectively.

Figures 5(a) and 5(b) plot the dissociation rates k_d and k_{off}, respectively, for two different values of interaction strength, ϵ, as a function of α, which sets the range of the potential (larger α results in a potential with a smaller range). Both k_d and k_{off} increase marginally with decreasing range but increase significantly when the interaction strength is halved. Decreasing range or the strength facilitates easier unbinding of the particles and hence increases the dissociation rate constants. Hence, the strength of the potential has a large influence on the dissociation rates.

Figures 5(c) and 5(d) show k_a and k_{on}, respectively, as a function of α, for two different values of interaction strength, ϵ. Here, k_a decreases by roughly a factor of two with decreasing range and only marginally when the interaction strength is halved. The effective rate constant k_{on} decreases only marginally with decreasing range and decreases even less when the interaction strength is halved. The range and the strength of the potential thus have a very small influence on the association rates.

Figure 5(e) shows the equilibrium constant computed from $K_{eq} = k_a/k_d = k_{on}/k_{off}$ as a function of α, for two different values of interaction strength, ϵ. For comparison, we included the values obtained from the analytical expression $K_{eq} = K_D^{-1} = 4\pi \int_0^{r_p} r^2 e^{-\beta V(r)} dr$. The simulations agree extremely well with the analytical expression.

B. Orientational distribution for the anisotropic potential

First, we determine how far from the σ-interface the orientational distributions of the particles become isotropic, as a function of the non-specific attraction strength, ϵ_{ns}. We determine this interface using two approaches: (i) Constructing the orientational distributions of the particles and checking at which interface these distributions become isotropic. (ii) Identifying the interface at which the value of k_{on}, calculated from Eq. (14), converges to a constant value.[24]

The orientational distributions are constructed from an extensive brute force BD simulation of two particles initially in the bound state. As the simulation progresses, the particles move away from each other. The position and orientation of the particles are recorded each time they cross one of the FFS interfaces at position r beyond the potential cutoff distance σ. The orientation is monitored via two parameters: (1) the angle θ between the inter-particle vectors at the initial bound state and the particles' current position and (2) the angle α between the patch vectors of the two particles. These two angles are illustrated at the top of Fig. 6. The remainder of Fig. 6 plots the probability distributions for the angle θ (left column) and of the angle α (right column) for five interfaces $R = 1.7, 1.9, 2.1, 2.3\sigma_{an}$. The interface where the angular distributions become

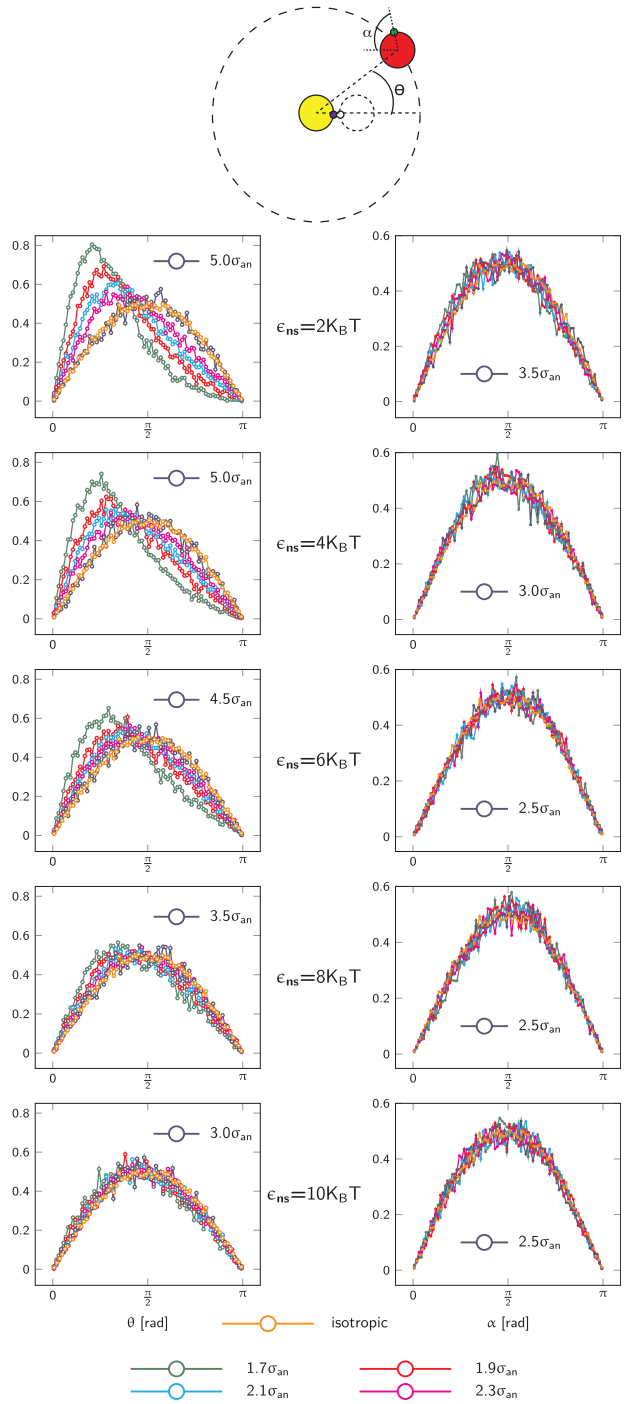

FIG. 6. The distributions of angles θ (left) and α (right) at different interfaces. θ is the angle between the initial (bound state) centre-of-mass vector and the centre-of-mass vector when the particle reaches the interface. α is the angle between the patch vector of the particle at the initial bound state and the patch vector when the particle reaches the interface. These angles are illustrated in the cartoon at the top of the figure. We see that the distribution of α becomes isotropic faster than the distribution of θ for any given ϵ_{ns}.

isotropic is indicated in grey; a distribution is considered to be isotropic when it qualitatively matches with the isotropic distribution. The isotropic distribution is plotted in orange for the sake of comparison. The peak in the θ distributions is shifted to lower angles for relatively small values of non-specific attraction strength ϵ_{ns} at interfaces near the bound state, due to a strong correlation with the initial orientation. At interfaces further away, due to diffusion and the truncation of the potential, particles are less correlated to the initial orientation and position and are eventually isotropically distributed. However, for larger values of the non-specific attraction strength, ϵ_{ns}, the distribution of θ becomes isotropic already at interfaces close to the bound state. This loss of correlation is caused by particles lingering longer in the non-specifically bound state and not immediately diffusing away. The probability distribution of α in the right column of Fig. 6 becomes isotropic at interfaces closer to the bound state when compared to the distribution of θ for the same non-specific attraction strength, ϵ_{ns}. We also observe that with increasing ϵ_{ns}, the shift in the interface where the orientational distributions α become isotropic does not shift as drastically as for the distributions of θ.

C. Rate constants for the anisotropic potential

Next, we study the behaviour of the rate constants by increasing the non-specific attraction strength ϵ_{ns}. We calculate the rate constants as explained in Sec. II A. As discussed above, it is important to determine the interface at which the orientational distributions become isotropic so that the expressions of the association rate constants are valid for anisotropic potentials. This can either be done by plotting the orientational distributions (see Sec. III B and Fig. 6) or by calculating $k_{\mathrm{on}}(\sigma')$ and determining the value of σ' for which the effective association rate becomes independent of σ' and reaches a constant. To this end, we computed $k_{\mathrm{on}}(\sigma')$ as a function of σ' using Eq. (14), for ten different values of the non-specific interaction strength ϵ_{ns}, see Fig. 7(a). We observe that as ϵ_{ns} increases, the value of k_{on} increases. We also notice that for interfaces close to the bound state, Eq. (14) predicts incorrect values for k_{on}. However, as we move further away, the orientational distributions become isotropic and k_{on} converges to the correct value. To quantitatively determine the interface where the value of k_{on} converges to the correct value, we calculate the relative error in k_{on}. The relative error in k_{on} is given by

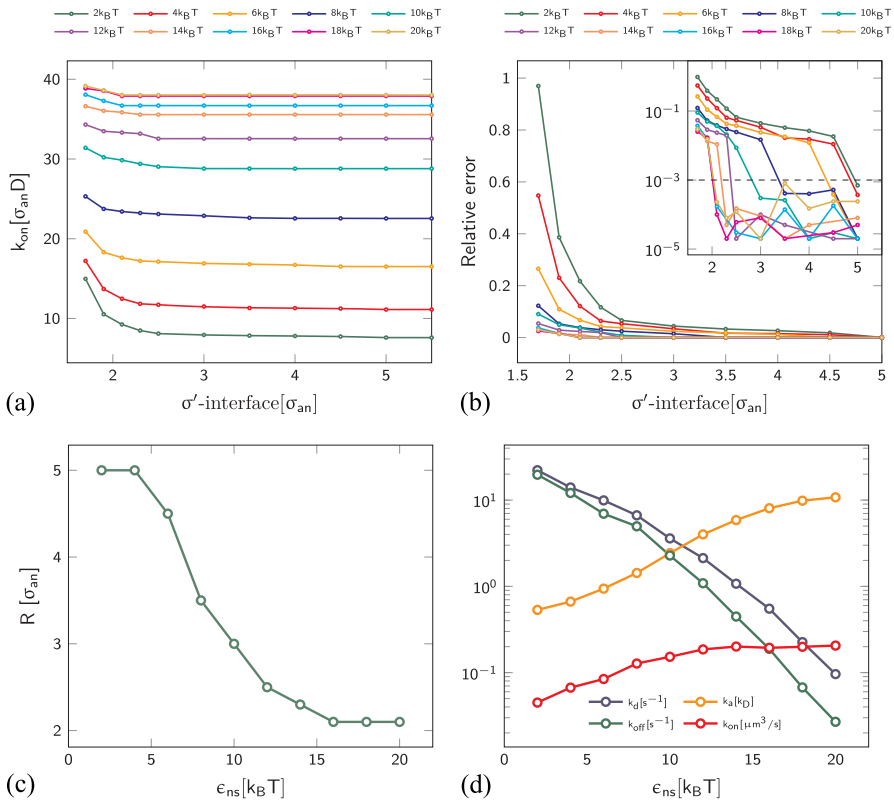

FIG. 7. The rates of association and dissociation for the anisotropic interaction potential. (a) k_{on} calculated from Eq. (14) as a function of the position of the σ'-interface, plotted for ten different values of the non-specific attraction strength, ϵ_{ns}. The value of k_{on} increases with increasing ϵ_{ns}. The plot shows k_{on} converging to the correct value as we move σ' further from the bound state. This is because Eq. (14) is valid only if the orientational distributions are isotropic in the interface where we measure k_{on} (b) The relative error in evaluating k_{on} as a function of σ'. At the interface where the value of k_{on} becomes a constant, the orientational distributions become isotropic. To determine this interface, we calculated the relative error $\frac{k_{\mathrm{on}}(\sigma')}{k_{\mathrm{on}}(5.5\sigma_{\mathrm{an}})} - 1$. If this relative error is below 0.01%, we conclude that k_{on} has converged. The inset shows the same plot in a semi-log scale. The dashed line denotes 0.1% relative error. (c) The interface at which the value of k_{on} becomes a constant as a function of the non-specific attraction strength ϵ_{ns}. The orientational distributions become isotropic at smaller distances for higher ϵ_{ns} because the particles spend more time near each other and have more time to decorrelate from the bound state configuration. (d) k_{a}, k_{d}, k_{on}, and k_{off} as a function of the non-specific attraction strength. k_{off} and k_{d} decrease significantly with increasing ϵ_{ns}. The k_{on} and k_{a}, on the other hand, increase initially with increasing non-specific attraction strength but later levels off. The increase in the association rates for a potential with ten times stronger ϵ_{ns} is one order of magnitude.

$\frac{k_{on}(\sigma')}{k_{on}(5.5\sigma_{an})} - 1$, where $k_{on}(\sigma')$ is the value of at a given interface σ' and $k_{on}(5.5\sigma_{an})$ is the value at the interface at $R = 5.5\sigma_{an}$. Figure 7(b) shows this relative error plotted as a function of the σ'-interface for ten different values of ϵ_{ns}. We assume that if the relative error is smaller than 0.1%, the value of k_{on} has converged to the correct value and at this point, we predict that the orientational distributions become isotropic. The interface value where $k_{on}(\sigma')$ converges is plotted as a function of ϵ_{ns} in Fig. 7(c). For a smaller value of ϵ_{ns}, particles need to move further away from the bound state for the value of k_{on} to converge. For a larger value of ϵ_{ns}, k_{on} converges at smaller distances since the particles stay longer in the nonspecific state, before diffusing away. We also predict that when k_{on} converges, the orientational distributions become isotropic. Indeed, the interface where the distribution of θ becomes isotropic as shown in Fig. 6 matches with the interface where the value of k_{on} converges as shown in Fig. 7(c).

Finally, Fig. 7(d) shows the behaviour of all the four converged rate constants as a function of ϵ_{ns}, evaluated at a cross section $\sigma = 1.6\sigma_{an}$. The intrinsic rates k_a were computed using Eq. (13). The dissociation rate constants k_d and k_{off} decrease with increasing ϵ_{ns}. In contrast, k_a and k_{on} increase initially with increasing ϵ_{ns} because the non-specific attraction promotes specific binding, as particles stay in each others vicinity. The increase in the association rates is not dramatic with increasing non-specific attraction strength: about an order of magnitude for a ten times increase in non-specific attraction strength. This behavior was also found in Ref. 35. Moreover, beyond a limiting value of ϵ_{ns}, the association rates reach a plateau. This is clearly caused by a flattening of the intrinsic association rate constant. This raises the question, whether the intrinsic rate constant can ever become very high, as is assumed in many diffusion influenced rate theories.

IV. DISCUSSION AND CONCLUSIONS

In this work, we have evaluated intrinsic and effective rate constants using the explicit microscopic expressions that we presented in Ref. 24. Knowledge of these rates is important to study the microscopic dynamics of reaction-diffusion systems. Furthermore, to construct Markov state models of reaction-diffusion systems, these rates are essential input parameters. Here we studied these rates in the context of an isotropic and an anisotropic potential. In the case of the isotropic potential, we evaluated these rates as a function of the range and the strength of the potential. We observed that the dissociation rates increase slightly as the interaction range is decreased yet increases drastically when the strength of the potential is halved. On the other hand, the association rates decrease with decreasing range. The change in the effective association rate constants is not significant.

In case of the anisotropic potential, we studied the behaviour of these rates as a function of the non-specific isotropic attraction. In addition to the bound and unbound states, this non-specific attraction facilitates a third non-specifically bound state in which the particles are attracted to each other, but not strongly bound to a particular patch. This increases the possibility of the particles to realign and bind at a specific patch, before diffusing away. The expression for the rates that we derived holds only if the orientational distributions of the particles are isotropic at the cross section where the rates are measured. We determined this interface directly from two angular distributions of the particles and by calculating the effective association rate as a function of the interface and identifying where this rate constant is converged. The interfaces obtained from both methods agree with each other. Knowledge of the location of this interface becomes important when we use the computed intrinsic rates to construct a Markov state model and combine them with the mesoscopic Green's function reaction dynamics method within a multi-scale scheme.[23,25]

The simulations also reveal that the dissociation rate decreases drastically when the non-specific isotropic attraction strength is increased (see Fig. 7). This is because non-specific binding increases the likelihood that particles that have just dissociated rebind instead of diffusing away. The association rate increases with the non-specific isotropic attraction strength. Non-specific binding keeps the particles that have diffused toward one another in close proximity, giving them time to align their patches and bind specifically. This effect is akin to the antenna effect in the binding of transcription factors to their specific sites on the DNA:[36] non-specific binding increases the effective cross section for the binding of proteins to their specific site. Our simulations also show that the effect of non-specific binding on the association rate is much weaker than that on the dissociation rate: while the effective and intrinsic dissociation rates decrease by more than two orders of magnitude when the non-specific interaction strength ϵ_{ns} is increased from $2k_BT$ to $10k_BT$, the effective association rate increases by less than an order of magnitude.[35] Moreover, while the effective dissociation rate continues to decrease as ϵ_{ns} is increased, the effective association rate saturates. This is because the overall association rate becomes increasingly limited by diffusion. Indeed, the intrinsic association rate continues to increase with ϵ_{ns}, although a close inspection of Fig. 7 shows that this rise levels off too—also the intrinsic association ultimately becomes limited by diffusion.

Many reactions are believed to be diffusion limited. This means that the intrinsic rate k_a is much higher than the diffusion-limited arrival rate k_D. Yet, how much larger the intrinsic rate can be, has, to our knowledge, not been systematically addressed before. Addressing this question, it should first be realized that the values of both k_a and k_D depend on the choice of the cross section σ: the larger σ, the larger the diffusion-limited arrival rate k_D and the lower the intrinsic rate k_a. However, a natural choice for σ is the distance as given by the effective physical size of the particles. After all, the intrinsic rate is typically interpreted as the rate at which the particles react given that they are in contact. Moreover, a small cross section also facilitates the modelling of many-body reaction-diffusion systems—the larger the cross section, the more often three-body (and higher) interactions have to be taken into account. Yet, at the microscopic scale, there is no unique definition for what the effective physical size is: one choice is the distance where the particles start to repel each other; another is the range of the interaction potential. However, choosing the first option would violate the basic

assumption made in Eq. (1), namely, that the cross section has to be chosen beyond the potential cutoff. Fortunately, for proteins interacting via isotropic potentials, the range of the potential is typically short and hence the ambiguity in the definition is not critical. The natural choice for σ is therefore the range of the interaction potential or more specifically its cutoff. This also means that the intrinsic association rate k_a cannot be made arbitrarily large but has an upper limit. This maximally achievable value of k_a will also depend on the shape of the isotropic potential. For instance, replacing the potential with a square well potential, of the same depth, while keeping the equilibrium constant K_{eq} fixed, moves the potential cutoff to lower values, with a corresponding higher k_a. For the isotropic Lennard Jones-based systems considered in this work, the intrinsic rate k_a, computed for a cross section σ given by the cutoff of the potential, is about a factor 1-10 higher than the diffusion-limited rate k_D. Thus, while these systems are in the diffusion-limited regime, they are still influenced by the intrinsic association rate k_a.

For particles interacting via anisotropic potentials, the interaction range is short for a given orientation of the particles. However, the distance beyond which the orientational distribution of the dissociating particles has become isotropic is much longer (see Fig. 6). It then follows from detailed balance that also the distribution of associating particles (more specifically, the distribution of trajectories that start in the unbound state and end in the bound state) become isotropic only beyond this distance. In this regime, one can truly speak of one well-defined intrinsic rate $k_a(\sigma)$, one diffusion-limited arrival rate $k_D(\sigma)$, and one cross section σ, independent of the orientation of the particles. However, as our earlier work[24] and that of Northrup *et al.*[2,29] show, it is still possible to talk about intrinsic association rate constants for cross section values that are smaller than the distance where the orientational distribution of association and dissociation trajectories becomes isotropic. These intrinsic rate constants should then be viewed as an average over all orientational dependent intrinsic rates. Indeed, as long as σ is chosen beyond the cutoff of the potential, our approach, via Eq. (13), does also make it possible to obtain k_a and k_D in this regime where the distribution of association/dissociation trajectories has not become isotropic yet.

Since the ratio k_a/k_D increases with decreasing σ, to address the maximal value of k_a/k_D, we thus compute k_a and k_D for the smallest possible choice of σ, which is again the cutoff of the potential. This ratio k_a/k_D depends on the strength of the non-specific attraction, see Fig. 7. When the non-specific attraction is weak, $k_a \approx 0.7k_D$, which means that association is reaction limited. This is because of the strong anisotropy of the interaction potential: the particles can only bind when their patches are properly aligned with each other, limiting the binding probability (of course, this reaction itself is also a diffusion process). Yet, the figure also shows that when ϵ_{ns} is increased, the intrinsic association rate increases. But it does not increase indefinitely. Instead k_a levels off, at a value that is on the order of 10 k_D [see Fig. 7(d)]. With $k_a \approx 10k_D$, the effective association rate is dominated by the diffusion-limited arrival rate yet still influenced by the intrinsic association rate.

It would also be of interest to study the effect of the shape of the potential on the values of the rates constant. For example, it would be of interest to compare the rates computed here for the modified LJ potential to those of a square-well potential. This comparison would then have to be performed on the footing of equal well-depth and equal range of the potential since this guarantees that the phase behaviour and the equilibrium constants are very similar. We leave this for future work.

Finally, we touch upon some apparent similarities and differences between our work and the Marcus theory for electron transfer.[37,38] Also in the Marcus theory, there is a diffusion-limited rate constant describing the rate of diffusion of the reactants until contact, and a intrinsic rate constant that describes the reaction.[38] However, the main difference with our approach is that in the Marcus theory the intrinsic rate constant describes the chemical electron transfer reaction rate, while in our description, the intrinsic rate constant k_a refers to the association given that the particles are at contact. Concomitantly, in the Marcus theory, the diffusion-limited rate constant describes the rate of diffusion into the potential well, while in our description, it describes the rate of diffusion up to the range of the potential. In the Marcus theory, the intrinsic rate constant can thus be higher because the chemical reaction rate can be much higher than the rate of diffusing into the potential well starting from the potential-cut-off; moreover, in that theory the diffusion-limited rate constant is lower because it describes the rate of diffusion into the potential well rather than merely to the edge of the well, as in our theory. The difference with the Marcus theory is thus mainly due to different definitions of the respective quantities. It would be interesting to see whether one could use the electron transfer reaction rate constant from the Marcus theory in combination with an intrinsic association rate constant and a diffusion-limited rate constant as defined here, to describe the kinetics of the entire process.

ACKNOWLEDGMENTS

This work is part of the Industrial Partnership Programme (IPP) "Computational sciences for energy research" of the Foundation for Fundamental Research on Matter (FOM), which is financially supported by the Netherlands Organization for Scientific Research (NWO). This research programme is co-financed by Shell Global Solutions International B.V.

[1] N. Agmon and A. Szabo, J. Chem. Phys. **92**, 5270 (1990).
[2] S. H. Northrup and H. P. Erickson, Proc. Natl. Acad. Sci. U. S. A. **89**, 3338 (1992).
[3] H.-X. Zhou, J. Chem. Phys. **108**, 8139 (1998).
[4] J. S. van Zon, M. J. Morelli, S. Tanase-Nicola, and P. R. ten Wolde, Biophys. J. **91**, 4350 (2006).
[5] K. Kaizu, W. de Ronde, J. Paijmans, K. Takahashi, F. Tostevin, and P. R. ten Wolde, Biophys. J. **106**, 976 (2014).
[6] K. Takahashi, S. Tănase-Nicola, and P. R. ten Wolde, Proc. Natl. Acad. Sci. U. S. A. **107**, 2473 (2010).
[7] I. V. Gopich and A. Szabo, Proc. Natl. Acad. Sci. U. S. A. **110**, 19784 (2013).
[8] K. Aokia, M. Yamada, K. Kunida, S. Yasuda, and M. Matsuda, Proc. Natl. Acad. Sci. U. S. A. **108**, 12675 (2011).
[9] H. C. Berg and E. M. Purcell, Biophys. J. **20**, 193 (1977).
[10] W. Bialek and S. Setayeshgar, Proc. Natl. Acad. Sci. U. S. A. **102**, 10040 (2005).

[11] K. Wang, W.-J. Rappel, R. Kerr, and H. Levine, Phys. Rev. E **75**, 061905 (2007).
[12] A. M. Berezhkovskii and A. Szabo, J. Chem. Phys. **139**, 121910 (2013).
[13] P. R. ten Wolde, N. B. Becker, T. E. Ouldridge, and A. Mugler, J. Stat. Phys. **162**, 1395 (2016).
[14] S. H. Northrup, J. Phys. Chem. **92**, 5847 (1988).
[15] G. Tkačik and W. Bialek, Phys. Rev. E **79**, 051901 (2009).
[16] J. Paijmans and P. R. ten Wolde, Phys. Rev. E **90**, 032708 (2014).
[17] B. A. Bicknell, P. Dayan, and G. J. Goodhill, Nat. Commun. **6**, 7468 (2015).
[18] J. S. van Zon and P. R. ten Wolde, J. Chem. Phys. **123**, 234910 (2005).
[19] M. J. Morelli and P. R. ten Wolde, J. Chem. Phys. **129**, 054112 (2008).
[20] J. Lipková, K. C. Zygalakis, S. J. Chapman, and R. Erban, J. Appl. Math. **71**, 714 (2011).
[21] M. E. Johnson and G. Hummer, Phys. Rev. X **4**, 031037 (2014).
[22] H. C. R. Klein and U. S. Schwarz, J. Chem. Phys. **140**, 184112 (2014).
[23] A. Vijaykumar, P. G. Bolhuis, and P. R. ten Wolde, J. Chem. Phys. **143**, 214102 (2015).
[24] A. Vijaykumar, P. G. Bolhuis, and P. R. ten Wolde, Faraday Discuss. **195**, 421 (2016).
[25] A. Vijaykumar, T. E. Ouldridge, P. R. ten Wolde, and P. G. Bolhuis, J. Chem. Phys. **146**, 114106 (2017).
[26] P. R. ten Wolde and D. Frenkel, Science **277**, 1975 (1997).
[27] F. C. Collins and G. E. Kimball, J. Colloid Sci. **4**, 425 (1949).
[28] O. G. Berg, Chem. Phys. **31**, 47 (1978).
[29] S. H. Northrup, S. A. Allison, and J. A. McCammon, J. Chem. Phys. **80**, 1517 (1984).
[30] J. S. van Zon and P. R. ten Wolde, Phys. Rev. Lett. **94**, 128103 (2005).
[31] T. S. van Erp, D. Moroni, and P. G. Bolhuis, J. Chem. Phys. **118**, 7762 (2003).
[32] R. J. Allen, P. B. Warren, and P. R. ten Wolde, Phys. Rev. Lett. **94**, 018104 (2005).
[33] R. J. Allen, C. Valeriani, and P. R. ten Wolde, J. Phys.: Condens. Matter **21**, 463102 (2009).
[34] R. Davidchack, T. Ouldridge, and M. Tretyakov, J. Chem. Phys. **142**, 144114 (2015).
[35] A. C. Newton, J. Groenewold, W. K. Kegel, and P. G. Bolhuis, J. Chem. Phys. **146**, 234901 (2017).
[36] T. Hu, A. Y. Grosberg, and B. I. Shklovskii, Biophys. J. **90**, 2731 (2006).
[37] R. A. Marcus, Rev. Mod. Phys. **65**, 599 (1993).
[38] R. A. Marcus and P. Siders, J. Phys. Chem. **86**, 622 (1982).